 DOI 10.1515/secm-2013-0156 — Sci Eng Compos Mater 2014; 21(4): 485–492

Cinzia Toscano, Aniello Riccio*, FrancescoPaolo Camerlingo and Carosena Meola

On the use of lock-in thermography to monitor delamination growth in composite panels under compression

Abstract: The success of composites in automotive, aerospace, and naval applications is mainly related to their aptitude to be tailored to obtain a final product that perfectly fulfills the design requirements. However, during both manufacturing processes and maintenance, some flaws, like delaminations (which may escape simple visual inspection), may be induced in composite structures. The presence of delaminations is of major concern for the load-carrying capability of carbon fiber-reinforced polymer panels. Indeed, delaminations can strongly affect the structural strength and may grow under in-service loads, leading sometimes to catastrophic failures. The aim of this work is to explore the use of lock-in thermography for the monitoring of delamination propagation in composite structures when subjected to generic multiaxial loading conditions. A stiffened composite panel with an embedded skin delamination subjected to compressive loading was taken as a benchmark to assess experimentally the effectiveness of lock-in thermography for monitoring the delamination propagation *in situ* during the compressive mechanical test. The delamination size as a function of the applied load, observed by lock-in thermography during the execution of the compressive test, was used to validate the results of preliminary numerical computations.

Keywords: buckling; CFRP; composites; delamination; lock-in thermography.

***Corresponding author: Aniello Riccio,** Department of Industrial and Information Engineering, Second University of Naples, Via Roma n 29, 81031 Aversa, Italy, e-mail: Aniello.riccio@unina2.it
Cinzia Toscano: Italian Aerospace Research Centre (CIRA), Via Maiorise sn, 81043 Capua, Italy
FrancescoPaolo Camerlingo: Alenia Aermacchi, Viale dell'Aeronautica, 80038 Pomigliano d'Arco, Naples, Italy
Carosena Meola: Department of Aerospace Engineering, University of Naples "Federico II", Via Claudio, n 21, 80100 Naples, Italy

1 Introduction

Carbon fiber-reinforced plastic (CFRP) composites are nowadays largely used in the aeronautical industry to manufacture primary and secondary aircraft parts. The CFRP appeal is related to the possibility to minimize structural weight and, hence, fuel consumption, leading to a significant reduction of costs and CO_2 emissions. Production processes [1] involve several parameters; therefore, a nonoptimized procedure could lead to final parts with enclosed intrinsic defects, such as delaminations. This type of defect could also be caused by low-energy impacts due to either tools dropping during maintenance or debris rising during aircraft takeoff and landing. Low-energy impacts can cause barely visible damages, whereas severe and complex delamination may be buried deep in the thickness of the impacted structure. This makes components more vulnerable to failure by buckling under a combination of compression, shear, and in-plane bending [2]. In particular, buckling loads may be substantially compromised by the presence of damage (up to 30% in the case of delamination [3, 4].

Big efforts have been dedicated to the development of effective nondestructive evaluation (NDE) techniques for the damage assessment and effective approaches for the continuous monitoring of structural integrity [5, 6], especially for aircraft and spacecraft parts. The most used conventional NDE [7, 8] techniques, such as ultrasonic C-scan, X-ray [9], and eddy current, generally require structural components of complex geometry to be disassembled during the inspection, which can be a time-consuming procedure. Hence, alternative approaches that can be used for continuous and *in situ* monitoring of real structures have been introduced.

One of the oldest methods for *in situ* monitoring is based on surface-bonded resistive foil strain gauges; however, it has been demonstrated to be ineffective for the monitoring of inner delamination. Generally, techniques able to detect unseen damage, preferably *in situ*, are regarded as structural health monitoring (SHM) systems. In particular, techniques often based on acoustic emission, which detects elastic waves emitted in the presence of damage growth under loading of the structure [10, 11], can be easily integrated into composite structures to create the so-called smart composite structures.

For SHM applications, embedded fiber optic sensors are very promising [12–14] even if some issues related to

the embedding of optical fibers still exist [15]. Some of the limits of all the types of smart structures are related to the need to locate sensors/actuators near the region where damage occurs, due to the expected local and/or global changes in strength and stiffness. In addition, the introduction of sensors/actuators can induce a strong modification in the original material characteristics.

In this work, an alternative approach to monitor the damage evolution in composite structures under in-service loading conditions is investigated. The attention is focused on the unusual application, on composite structures subjected to a mechanical load, of a common NDE technique, such as lock-in thermography [16, 17]. This technique, based on thermal waves and recently promoted as a certified method for nondestructive testing of aeronautical components, is usually taken into account, especially for its contactless aspect, fast testing, and suitability for on-field applications. Indeed, pulsed phase thermography, which is an alternative NDE approach based on thermal waves, could be considered much more effective than lock-in thermography especially for detecting deep defects. However, for the application presented in this paper, lock-in thermography has been considered mainly because the investigated defect is not deep and because the data analysis software needed for lock-in thermography is generally provided by the thermal camera manufacturer (FLIR®); thus, no time-consuming work is required, only personnel training.

Lock-in thermography is nowadays commonly used to check the integrity of structures after an impact and a fatigue testing campaign. In the frame of the present work, this NDE technique has been used on an *ad hoc* manufactured delaminated stiffened composite panel, simultaneously to the application of a compression load, to track the evolution of the artificial delamination. With the depth of the defect known, the lock-in test has allowed monitoring of the size and shape of the defect in a very fast way (almost 30 s).

The applied compressive load was increased in discrete steps in order to carry out, between consecutive steps, a complete lock-in test to search for any modification of the artificial embedded delamination size until the failure of the panel.

By means of the obtained phase images, the realistic evolution of delamination with the onset of the delamination buckling and growth phenomena was observed. The obtained experimental results have been used for comparisons with numerical finite element-based tool outputs.

In this work, expertise from research centers, academy, and industry has been shared to gain novel information on the propagation of delamination in composites and to suggest a useful NDE methodology able to provide data on the delamination growth phenomenon to be used for the validation of sophisticated numerical models.

In Section 2, the chosen delaminated stiffened panel configuration and the numerical results on delamination growth under compressive loading conditions are introduced, and in Section 3, the experiments performed are described and the infrared thermography results are assessed.

2 Benchmark configuration and finite element method model predictions

The delaminated stiffened composite panel configuration, shown in Figure 1, was adopted as benchmark for the experimental activities on the monitoring of delamination growth under compression load described in the next section. The stacking sequence $[(+45°/0°/90°/-45°)_3]_S$ was used to manufacture the panel skin and the two L flanges used to create the T stringers. Furthermore, an embedded circular delamination was artificially created by means of a Teflon disk with a diameter of 40 mm, placed within the skin plies before curing. As mentioned previously, delaminations, which may arise as a consequence of manufacturing defects or due to low-velocity impacts, may grow under service loads, leading to a premature structural collapse. Indeed, under compression load, the delaminated layers can buckle following several buckling shapes (see Figure 2), which cause a consistent loss of structural strength.

It is well known, from the fracture mechanics of composites, that strain energy release rate rules the propagation of delaminations. For each fracture mode (opening mode I, forward shear mode II, and parallel shear mode III), a critical strain energy release rate, representative of the material toughness, can be defined.

Once these critical values of strain energy release rate for the basic fracture modes are known, from *ad hoc* experiments, it is possible to predict mixed mode delamination propagation in laminates by means of suitable criteria such as the power law criterion:

$$\left(\frac{G_{\mathrm{I}}}{G_{\mathrm{I_c}}}\right)^{\alpha}+\left(\frac{G_{\mathrm{II}}}{G_{\mathrm{II_c}}}\right)^{\beta}+\left(\frac{G_{\mathrm{III}}}{G_{\mathrm{III_c}}}\right)^{\gamma}=E_{\mathrm{d}}\geq 1 \tag{1}$$

The satisfaction of relation (1) is assumed to be the necessary condition for delamination growth.

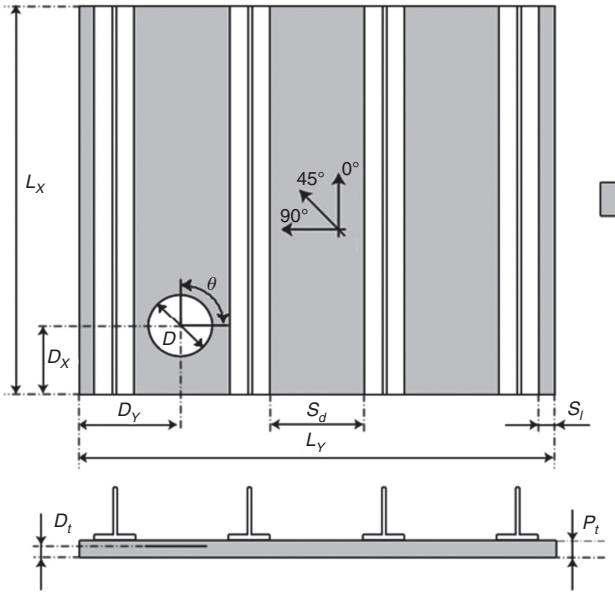

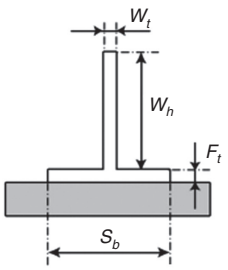

L_y	Panel length	600 mm
L_x	Panel width	475.8 mm
S_l	Dist. btw. panel edge and stringer foot	21 mm
S_d	Dist. btw. stringers	114. mm
S_b	Stringer foot width	54 mm
P_t	Skin thickness	2.8 mm
F_t	Stringer foot thickness	2.8 mm
W_h	Stringer web height	25.2 mm
W_t	Stringer web thickness	5 mm
D_y	Delamination position along length	131 mm
D_x	Delamination position along width	107 mm
D_t	Delamination depth	2.45 mm
D_D	Delamination diameter	40 mm

Property	AS4/3501-6	Description
E_{11}	147 GPa	Longitudinal Young's modulus
E_{22}	9 GPa	Transverse Young's modulus
$G_{12}=G_{13}$	5 GPa	Shear modulus
G_{23}	3 GPa	
$v_{12}=v_{13}$	0.3	Poisson's ratio
v_{23}	0.42	
G_{Ic}	175 J/m^2	Critical strain energy release rate for mode I
$G_{IIC}=G_{IIC}$	532 J/m^2	Critical strain energy release rate for mode II/mode III
T_p	0.117 mm	Ply thickness

Figure 1 Tested panel configuration with position of the artificial delamination.

The delamination growth phenomenon is usually modeled in numerical finite element codes by means of interface fracture elements, which use the virtual crack closure technique (VCCT) to calculate, along the delamination front, the strain energy release rate to be introduced in Eq. (1). According to the VCCT, the strain energy released by a crack growing from size a to $a+\Delta a$ is equal to the amount of work required to close the same crack from $a+\Delta a$ to a [18, 19]. Improved versions of the VCCT are being developed that can take into account the complex contact phenomena between sublaminates, the nonregular delamination fronts, and the dependence of strain energy release rate from the mesh size and the time increment [20–24]

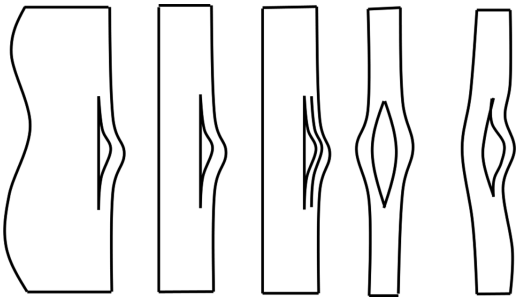

Figure 2 Possible delamination buckling shapes.

The finite element model was adopted to simulate the compressive behavior of the delaminated stiffened panel under consideration and implemented in ABAQUS™, using eight-node solid elements in the delaminated region with interface fracture elements at the delamination front. The rest of the panel was modeled by eight-node shell elements. The connections between solid and shell elements were performed by contact elements based on multipoint constraint (MPC) kinematic relations. The same approach was used to create shell-to-shell connections between the skin and the stringer feet. The resulting finite element method (FEM)-based model is shown in Figure 3.

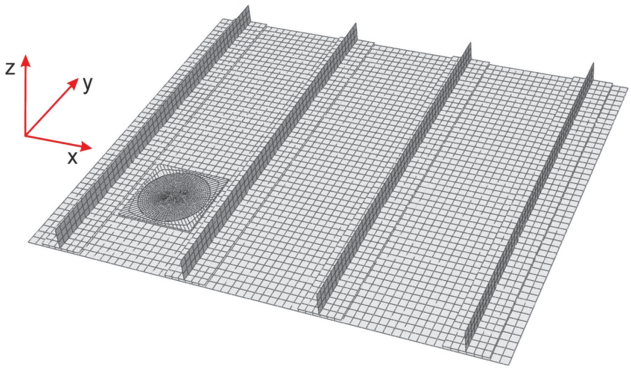

Figure 3 FEM model of the stiffened panel with the embedded artificial delamination at the lower left side.

The compressive load was applied along the *y* direction (see Figure 3), and the compression behavior of the panel in the delaminated area was evaluated in detail. In Figure 4, the delamination buckling is shown as a contour plot of the out-of-plane displacements, whereas in Figure 5, the delamination growth phenomenon is represented at different load levels of the geometrically nonlinear analysis.

In Figure 5 the buckling shape change is shown compared to the perimeter of the initial circular embedded delamination, which is highlighted by a red circle. In Figure 5A, representing the deformation obtained by loading the structure up to 300 kN, the delamination buckling phenomenon is clearly noticeable. In Figure 5B, the deformation reaches the boundary of the delaminated area for a compressive load of 450 kN. By increasing the load (up to 500 kN in Figure 5C and up to 600 kN in Figure 5D), the deformation of the buckled sublaminate extends beyond the initial delaminated area, indicating a marked propagation of the delamination. Due to the presence of ±45 oriented plies in the composite laminate, the delamination growth is characterized by an elliptical shape whose major axis has a direction not exactly perpendicular to the applied compression loading direction.

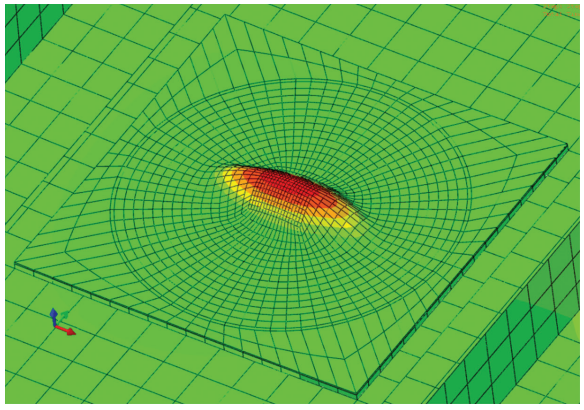

Figure 4 View of the delamination buckling.

3 NDE experimental results

Before the compression test was started, the panel was nondestructively inspected by means of a standard lock-in test.

The lock-in test is performed by heating the specimen with a modulated light while the thermal camera acquires the surface temperature variations. In this work, the reflection mode has been adopted, and the modulated halogen lamp and the thermal camera were positioned on the same side of the panel (see Figure 6).

The thermal energy delivered into the material propagates as thermal wave within it is partially reflected. The reflected wave interferes with the incoming one, producing an oscillating interference pattern that can be measured in terms of amplitude (representative of the amount of thermal energy transmitted to the material) and phase (phase delay between the delivered and the reflected thermal waves). The application of this method is based on the use of simple relations among the thermal diffusion length μ, the thermal diffusivity coefficient α, and the wave frequency $f=\omega/2\pi$, such as:

$$\mu=\sqrt{\frac{\alpha}{\pi f}} \tag{2}$$

Indeed, the thermal diffusion length μ is representative of the maximum depth at which effective amplitude images (representative of the material integrity and homogeneity status) can be taken. Effective phase images (representative of the homogeneity status and, eventually, of the depth of defects) can be taken up to about double the thermal diffusion length. For instance, the following relation, providing the maximum depth at which effective phase images can be taken, holds:

$$p=1.8\mu \tag{3}$$

Adopting Eq. (3), the diffusivity of a panel with known thickness can be easily calculated. In the present paper, the thermal diffusivity of the panel was evaluated by adopting a metal patch in contact with the rear side of the panel. The metal patch was used to determine the highest stimulation frequency that penetrates the composite panel by obtaining a phase image of the metal patch with an appreciable phase contrast $\Delta\phi$ between the homogeneous

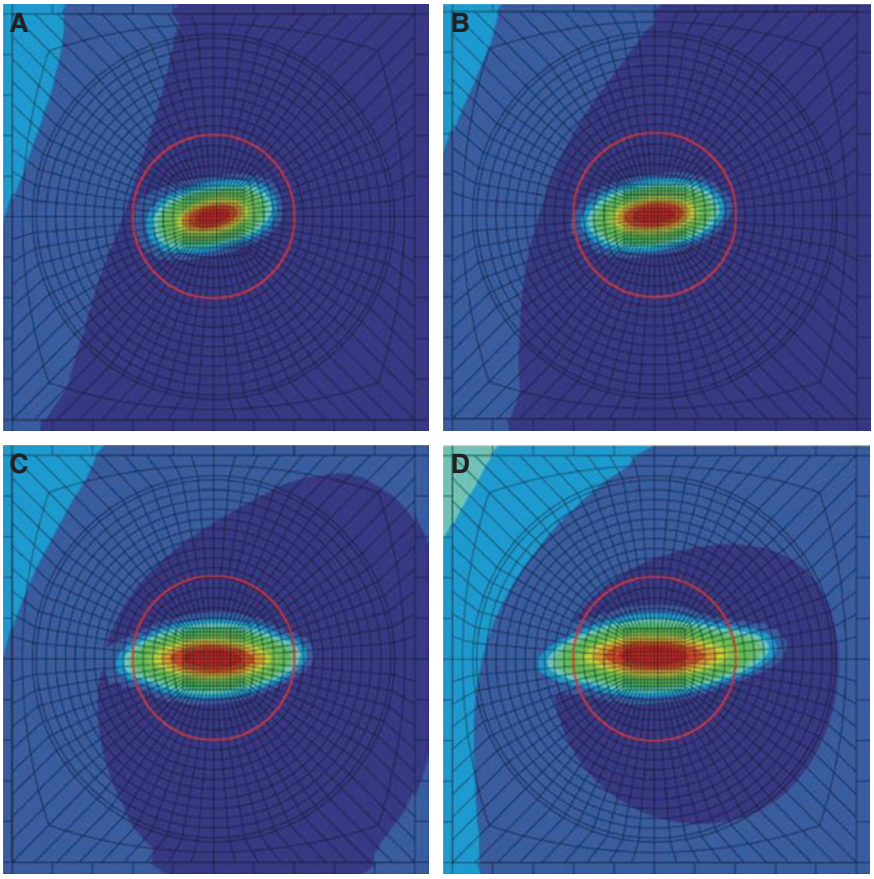

Figure 5 Evolution of the buckling of the delaminations during compression loading.

and the inhomogeneous regions. The phase contrast can be expressed by:

$$\Delta\phi=\frac{\phi_H-\phi_I}{\phi_H} \tag{4}$$

where ϕ_H and ϕ_I are the phase values of the homogeneous and the inhomogeneous area, respectively.

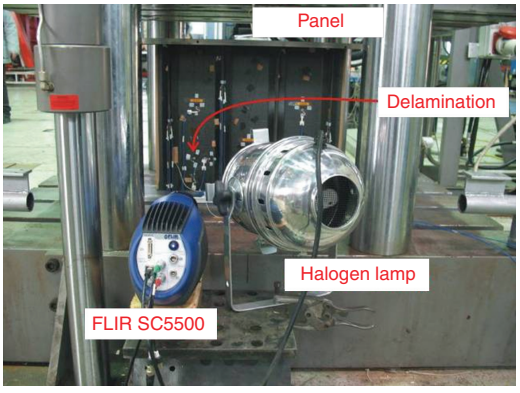

Figure 6 Setup for the nondestructive lock-in thermography tests.

Because the frequency was selected to provide p to be equal to the thickness of the composite panel L, the thermal diffusivity of the panel was obtained from Eqs. (2) and (3) as:

$$\alpha=\pi f\left(\frac{L}{1.8}\right)^2 \tag{5}$$

By this approach, the depth of defects embedded in CFRP panels can be evaluated once the diffusivity is known simply by tuning f.

The adopted lock-in procedure allowed us to detect the Teflon disk (located under the third ply with respect to the observed skin side) and to measure its diameter without the application of any compressive load.

With the stimulation frequency of 0.3 Hz, the best phase contrast was obtained. Thus, the real initial delamination diameter was easily measured on the phase map and was found to be 41 mm.

In the phase image, which is shown in Figure 7, the disk is highlighted by a blue dot; it can be noted that the Teflon disk appears to be not perfectly circular, with a very

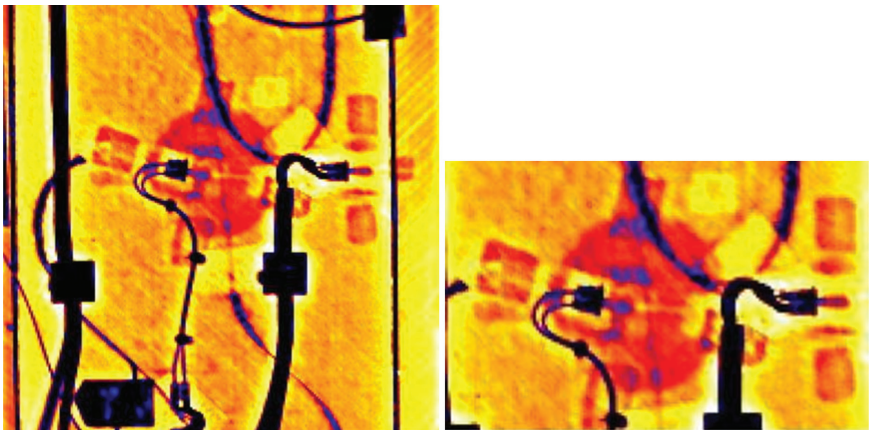

Figure 7 Phase image taken at 0.3 Hz stimulation frequency. A magnification of the embedded delamination can be seen on the right side with highlighting of the missed lower left part (blue arrow).

small missing portion in the right side as indicated by the blue arrow. This imperfection, likely to be ascribed to a possible crimp of the disk during the panel skin preparation, does not seem to have influenced the experimental results in terms of delamination growth.

The optimal parameters found with this preliminary lock-in inspection and used for all the next tests are summarized in Table 1.

After the preliminary lock-in thermography test, the stiffened panel was properly constrained in the MTS (Eden Prairie, MN, USA) servohydraulic fixture (see Figure 6), and a compression loading was gradually applied in 13 steps up to the panel failure.

At each step, corresponding to a certain load level, the progressive compression was paused to perform a lock-in test aimed to the monitoring of the delamination size and shape variations. The first phase image was taken at 100 kN and the last at 600 kN just before the panel failure.

Some of the phase images obtained for increasing values of the compression load are shown in Figure 8. In the phase map obtained at 315 kN, the onset of the delamination buckling can be appreciated thanks to the presence of the two lighter horizontal lines symmetrically placed in the central part of the embedded delamination. At 473 kN the delamination buckling reached the perimeter of the embedded delamination as numerically predicted (see Figure 5B). With increasing compression load, the delamination propagated in the horizontal direction as shown in Figure 8 at 523 and 600 kN. These last delamination configurations show a growth in agreement, respectively, with the numerical predictions represented in Figure 5C and D. This cross-comparison between experimental data and numerical results shows how the proposed NDE approach can be effectively adopted to obtain useful experimental data on delamination growth, which can endorse the validation of refined numerical models.

Table 1 Lock-in test parameters.

Parameter	Value
Halogen lamp stimulation frequency (Hz)	0.3
Frequency rate (thermal camera) (Hz)	111
Integration time (thermal camera) (μs)	1205
Acquired frames	1110

Indeed, the propagation becomes appreciable only at 473 kN. The horizontal delamination diameter at 523 kN is almost 49 mm, and it increases to about 54 mm at 600 kN.

The application of lock-in thermography during the test has allowed the monitoring of not only the delamination-related phenomena but also the onset of the global skin buckling in the stiffened panel. In fact, by comparing the phase images shown in Figure 8 for different load values with the one obtained without any loading (Figure 7), it can be noticed that the deformation of the panel surrounding the Teflon disk can also be obtained. It is worth noting that by means of the phase images, any displacement in the out-of-plane direction is represented by different colors, which correspond to different phase values. Comparing the phase images shown in Figures 7 and 8, the surface of the panel seems to first (before 523 kN) move out of plane far from the infrared camera, whereas it moves in the opposite direction for increased values of the compressive load.

4 Conclusions

In this paper, an alternative approach to monitor the delamination evolution in composite structures is

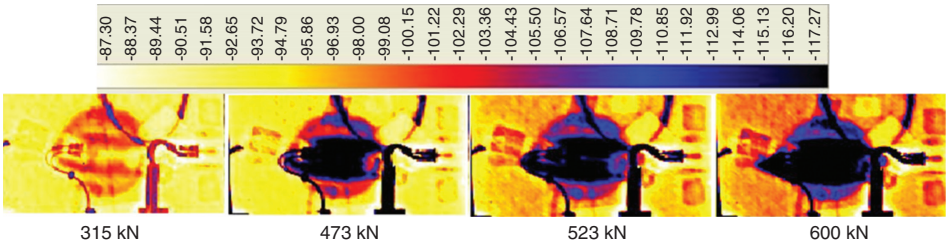

Figure 8 Phase images obtained at increasing compression loads. The buckling deformation and its propagation can be appreciated. The scale is referred to the phase angle expressed in degrees.

investigated. Indeed, lock-in thermography has been unusually used during the execution of a mechanical test to monitor the delamination evolution under real loading conditions.

A CFRP stiffened composite panel with an artificial embedded delamination was used as a benchmark to verify the effectiveness of the proposed NDE approach. The panel was subjected to a compression test by using a servohydraulic MTS machine, and the delamination growth was monitored by performing lock-in thermography tests at intermediate load steps without unloading the panel. The application of the compressive load during the mechanical test was paused 13 times to allow the NDE inspections.

The delamination buckling and growth were observed, quantifying the load levels triggering these phenomena. In addition, information on the skin global buckling phenomenon could be deduced by means of the produced phase images. Comparisons with results, in terms of delamination size as a function of the applied load, obtained by means of advanced numerical models available in commercial FEM codes, demonstrated the utility of this technique to provide brand-new experimental data representative of the damage status under in-service loads, which are needed for numerical model validation. Future work will be devoted to the tentative extension of the application of the proposed approach to the monitoring of intralaminar composite failure mechanisms (fiber breakage and matrix cracking) under in-service loading conditions.

Received July 9, 2013; accepted September 24, 2013; previously published online November 23, 2013

References

[1] Meola C, Toscano C. *Recent Pat. Mater. Sci.* 2012, 5, 48–67.
[2] Greenhalgh E, Singh S, Nilsson KF. *ASTM Spec. Tech. Publ.* 2000, 1383, 49–71.
[3] Abrate S. *Appl. Mech. Rev.* 1994, 47, 517–544.
[4] Greenhalgh E, Meeks C, Clarke A, Thatcher J. *Composites, Part A* 2003, 34, 623–633.
[5] Reid SR, Zhou G. *Impact Behaviour of Fibre-reinforced Composite Materials and Structures*, Woodhead Publishing: Cambridge, 2000.
[6] Culshaw B. *NDT Int.* 1985, 8, 265–273.
[7] Beine C, Boller C, Netzelmann U, Porsch F, Ramanan SV, Schulze M, Bulavinov A, Heuer H. NDT for CFRP aeronautical components – a comparative study. Paper presented at NDT in Aerospace, November 22–24, 2010, Hamburg, Germany.
[8] Maldague XPV. *Theory and Practice of Infrared Technology for Nondestructive Testing*. John Wiley & Sons, Inc.: New York, 2001.
[9] ASTM E976. A standard guide for determining the reproducibility of acoustic emission sensor response. American Society for Testing and Materials, West Conshohocken, PA 19428-2959, US, 1994.
[10] Surgeon M, Wevers M. *NDT&E Int.* 1999, 32, 311–322.
[11] Levin K, Nilsson S. *Proc. SPIE* 1996, 2779, 222–231.
[12] Riccio A, di Caprio F, Camerlingo F, Scaramuzzino F, Gambino B. *Appl. Compos. Mater.* 2013, 20, 73–86.
[13] Voto C, Inserra S, Camerlingo FP, Iodice M, Rendina I. Fiber optic strain sensors: aerospace applications and requirements. Paper presented at The First European Workshop for Structural Health Monitoring, July 10–12, 2002, Paris, France.
[14] Sirkis JS, Dasgupta A. In *Fiber Optic Smart Structures*, Eric Udd, Ed., Wiley: New York, 1995, pp. 61–107.
[15] Meola C, Carlomagno GM. In *Recent Advances in Non Destructive Inspection*, Carosena Meola, Ed., Nova Science Publisher Inc: New York, 2010, pp. 89–23.
[16] Busse G. In *Nondestructive Testing Handbook,* Maldague X, Ed., American Society for Nondestructive Testing Inc: Columbus, OH, 2001, Vol. 3, pp. 318–327.
[17] Meola C, Carlomagno GM, Squillace A, Vitiello A. *Eng. Failure Anal.* 2006, 13, 380–388.
[18] Riccio A, Perugini P, Scaramuzzino F. *Composites, Part B* 2001, 32, 209–218.
[19] Riccio A, Pietropaoli E. *Int. J. Compos. Mater.* 2008, 42, 1309–1335.
[20] Pietropaoli E, Riccio A. *Compos. Sci. Technol.* 2011, 71, 836–846.

[21] Pietropaoli E, Riccio A. *Appl. Compos. Mater.* 2011, 18, 113–125.
[22] Pietropaoli E, Riccio A. *Compos. Sci. Technol.* 2010, 70, 1288–1300.
[23] Riccio A, Raimondo A, Scaramuzzino F. *Appl. Compos. Mater.* 2013, 20, 465–488.
[24] Riccio A, Scaramuzzino F, Perugini P. *AIAA J.* 2003, 41, 933–940.